Liquid Structures and the Infrared and Isotropic/Anisotropic Raman Noncoincidence in Liquid Methanol, a Methanol−LiCl Solution, and a Solvated Electron in Methanol: Molecular Dynamics and ab Initio Molecular Orbital Studies

Hajime Torii*

Department of Chemistry, School of Science, The University of Tokyo, Bunkyo-ku, Tokyo 113-0033, Japan

Received: October 29, 1998; In Final Form: February 8, 1999

The relationship between the liquid structures, vibrational interactions, and the wavenumber differences among the infrared (IR), isotropic Raman, and anisotropic Raman components of vibrational bands (the noncoincidence effect) is analyzed theoretically for the OH stretching bands of neat liquid methanol and a methanol−LiCl solution. The analysis is also carried out for the CO stretching band of neat liquid methanol for comparison. The IR and Raman spectra are calculated on the basis of the transition dipole coupling (TDC) mechanism and the liquid structures derived from molecular dynamics (MD) simulations (the MD/TDC method). It is shown that the signs and magnitudes of the noncoincidence effect observed for the OH and CO stretching bands of liquid methanol, which are significantly different between these two bands, are well reproduced by the calculations based on the same set of liquid structures and the same mechanism of vibrational interactions. The analysis of the origin of the noncoincidence effect shows that the vibrational interactions within hydrogen-bonded chains explain the major part of the noncoincidence effect for the OH stretching band of liquid methanol, while in the case of the CO stretching band, the negative noncoincidence effect arising from the vibrational interactions between hydrogen-bonded molecules is partially canceled by the contribution of the interactions between molecules which are not directly hydrogen bonded to each other. The reversed (negative) noncoincidence effect observed for the OH stretching band of a methanol−LiCl solution is shown to be mainly explained by the liquid structures formed around the Cl^- ion and the vibrational interactions determined by the TDC mechanism. To support the discussion, ab initio molecular orbital (MO) calculations are performed for cluster species consisting of a Cl^- or Li^+ ion and a few methanol molecules. As an extension of the study on the methanol−Cl^- system, ab initio MO calculations are also carried out for clusters with an electron substituted for the Cl^- ion. A possible vibrational spectroscopic feature of the liquid structures formed around a solvated electron is discussed.

1. Introduction

The phenomenon that the wavenumbers of the infrared (IR), isotropic Raman, and anisotropic Raman components of a vibrational band do not coincide, called the noncoincidence effect, has been studied for the past decades. The C═O stretching band of liquid acetone is among the typical cases for which the noncoincidence effect can be clearly observed.[1−4] For this vibrational band, as well as the corresponding bands of other carbonyl compounds such as *N*,*N*-dimethylacetamide,[1,4,5] it has been observed that the isotropic Raman component is significantly lower in wavenumber than both the IR and anisotropic Raman components, with a smaller wavenumber difference between the latter two; i.e., $\nu_{iso} < \nu_{aniso} \cong \nu_{IR}$. This noncoincidence effect has been interpreted as arising from intermolecular vibrational interactions determined by the transition dipole coupling (TDC) mechanism.[6−9] The experimental results that the magnitude of the noncoincidence is reduced by isotopic and chemical dilution (e.g., dilution with acetone-^{18}O or CCl_4)[10−13] support this view. According to the TDC mechanism, a vibrational coupling constant depends on the distance and relative orientation of the molecules involved in the coupling.[6−9,14] It is therefore expected that the sign and the magnitude of the noncoincidence effect are sensitive to the liquid structure, particularly the relative orientation of neighboring molecules. When the liquid structure is determined by the interactions between permanent dipoles of molecules and if the permanent dipole is parallel to the transition dipole of the relevant vibration, an analytical theory[7] based on the mean spherical approximation[15] predicts the noncoincidence as $\nu_{iso} < \nu_{aniso} \cong \nu_{IR}$, in agreement with the experimental results obtained for the C═O stretching bands of liquid acetone and other carbonyl compounds.

When the liquid structure is mainly determined by hydrogen-bonding interactions, the relation $\nu_{iso} < \nu_{aniso} \cong \nu_{IR}$ does not necessarily hold even if the intermolecular vibrational interactions are determined by the TDC mechanism. The CO stretching band of liquid methanol[16] is among such cases. The isotropic Raman component of this vibrational band is observed at ∼1036 cm^{-1}, which is *higher* by 5 cm^{-1} than the anisotropic component (∼1031 cm^{-1}).[16] In our previous study,[8] this vibrational band has been analyzed on the basis of the TDC mechanism and the liquid structures derived from Monte Carlo (MC) simulations (the MC/TDC method). It has been shown that the observed Raman noncoincidence is explained by the TDC mechanism

* Phone and fax: +81-3-3818-4621. E-mail: torii@chem.s.u-tokyo.ac.jp.

10.1021/jp9842650 CCC: $18.00
Published on Web 03/20/1999

and is consistent with the relative orientation of the CO bonds of methanol molecules determined by intermolecular hydrogen bonding.

In liquid methanol, the noncoincidence effect can be observed also for the OH stretching band.[17,18] In contrast to the case of the CO stretching band, the wavenumber of the isotropic component ($\sim$3320 cm^{-1}) of the OH stretching band is *lower* than that of the anisotropic component ($\sim$3380 cm^{-1}). In this respect, the situation may seem to be similar to that of the C=O stretching band of liquid acetone, although the magnitude of the noncoincidence is significantly different (60 cm^{-1} for the OH stretch of methanol vs 5 cm^{-1} for the C=O stretch of acetone). The feature that is unique to the OH stretch of methanol is that the IR band (3350 cm^{-1})[19] comes near the middle of the two Raman components, i.e., $\nu_{iso} < \nu_{IR} < \nu_{aniso}$. It is therefore interesting to examine whether the liquid structure of methanol derived from numerical simulations is consistent with this experimental result.

When lithium chloride or lithium bromide is dissolved in liquid methanol, the OH stretching band is affected significantly.[18,20] The wavenumber separation between the two Raman components, denoted $\Delta\nu_{aniso-iso}$ ($=\nu_{aniso} - \nu_{iso}$), which is positive for neat liquid methanol, is reduced as the concentration increases and becomes negative above a certain concentration. At the LiCl/methanol mole ratio of 0.18,[18] $\Delta\nu_{aniso-iso}$ is -44 cm^{-1}, which is different from that of neat methanol by about 100 cm^{-1}. Two different mechanisms have been proposed to explain this experimental result. Perchard[20] has suggested that this reversed Raman noncoincidence originates from a tetrahedral arrangement of methanol molecules around the halide ion, the vibrational interactions among which being determined by the TDC mechanism. By contrast, Kecki and Sokolowska[18,21] have suggested that indirect vibrational interactions between methanol molecules mediated by the polarization of the metal ion and/or the halide ion,[22] rather than direct vibrational interactions, give rise to the negative Raman noncoincidence for the methanol−LiCl solution and some other electrolyte solutions. It is therefore interesting to analyze the microscopic liquid structures around the ions by numerical simulations and to examine whether direct vibrational interactions of molecules around the ions give rise to the observed feature of the OH stretching Raman band.

In the present study, the IR and isotropic/anisotropic Raman noncoincidence has been analyzed theoretically for the OH stretching bands of neat liquid methanol and a methanol−LiCl solution. For neat liquid methanol, the analysis is based on the TDC mechanism and the liquid structures derived from molecular dynamics (MD) simulations (the MD/TDC method). The relation between the relative orientation of neighboring molecules in the liquid and the vibrational spectral features is examined. The results are compared with those obtained for the CO stretching band. The analysis for a methanol−LiCl solution is carried out with the following two methods: (1) the MD/TDC method based on the results of MD simulations on methanol−Cl^- and methanol−Li^+ solutions and (2) ab initio molecular orbital (MO) calculations on cluster species consisting of a few methanol molecules and a Cl^- or Li^+ ion. The liquid structures, vibrational interactions, and vibrational motions responsible for the spectral features are clearly shown. As an extension of the study on the methanol−Cl^- system, ab initio MO calculations are also carried out on a few cluster species with an electron substituted for the Cl^- ion. The IR−Raman noncoincidence characteristic of liquid structures formed around a solvated electron is predicted on the basis of these calculations.

2. Computational Procedure

A. Calculations of the Structures and Vibrational Spectra of Neat Liquid Methanol by the MD/TDC Approach. MD simulations were performed on neat liquid methanol by using a polarizable intermolecular potential function derived by Gao et al.,[23] in which many-body interactions are taken into account by assuming isotropic polarizability on all the atoms. Intermolecular forces due to induced dipoles were calculated by the method described in ref 24. Only intermolecular degrees of freedom were considered. Four-dimensional vectors (quaternions) were used to represent molecular orientations in solving the equations of motion,[25,26] in combination with the leapfrog integration method.[26] The liquid system consisted of 216 molecules in a cubic cell. The periodic boundary condition was employed. The volume of the cubic cell was fixed so that the molecular volume is equal to that given in ref 23. The temperature was kept at 298 K by adjusting the total kinetic energy every 200 fs. The time step was set to 2 fs. The system was equilibrated for 64 ps, after which a production run of 80 ps was carried out.

IR and Raman spectra were calculated by treating each molecule as an oscillator having a transition dipole, in the same way as in our previous studies.[8,12,27,28] Liquid structures were extracted from the MD simulation (the production run of 80 ps) every 200 fs, and the IR and Raman spectra calculated for such 400 instantaneous liquid structures were averaged. All the diagonal elements of the **F** matrix were assumed to be 6.75 mdyn Å^{-1} amu^{-1} for the OH stretch and 0.627 mdyn Å^{-1} amu^{-1} for the CO stretch, which correspond to an unperturbed vibrational wavenumber of 3385 and 1032 cm^{-1}, respectively. The off-diagonal elements were determined by the TDC mechanism, and are expressed as

$$F_{ij} = \frac{\delta\boldsymbol{\mu}_i \delta\boldsymbol{\mu}_j - 3(\delta\boldsymbol{\mu}_i \mathbf{n}_{ij})(\delta\boldsymbol{\mu}_j \mathbf{n}_{ij})}{R_{ij}^3} \quad (1)$$

where $\delta\boldsymbol{\mu}_i$ and $\delta\boldsymbol{\mu}_j$ are the transition dipoles of the relevant vibrations of molecules i and j, $\mathbf{n}_{ij}$ is the unit vector along the line connecting the two transition dipoles, and R_{ij} is the distance between the two transition dipoles. The normal modes of the liquid system were calculated by diagonalizing the **F** matrix (with size 216 × 216) thus constructed. The vibrational transition dipole of each molecule, with a magnitude of 3.647 D Å^{-1} amu$^{-1/2}$ (OH stretch) or 1.54 D Å^{-1} amu$^{-1/2}$ (CO stretch), was assumed to be parallel to, and located at the center of, the relevant (OH or CO) bond. The magnitude of the transition dipole is consistent with the observed IR intensities.[29,30] The Raman tensor of each molecule was assumed to be axially symmetric with respect to the relevant bond. Each calculated spectrum was convoluted with a Gaussian function with a half-width at half-maximum of 60 cm^{-1} (OH stretch) or 9 cm^{-1} (CO stretch) to take into account band broadening due to factors other than TDC.

These calculations were carried out on an NEC SX-3R supercomputer at the Computer Center of the Institute for Molecular Science and on an S-3800 supercomputer at the Computer Center of the University of Tokyo.

B. Calculations of the Structures and Vibrational Spectra of Methanol−Cl^- and Methanol−Li^+ Solutions by the MD/TDC Approach. MD simulations on these solutions were performed by substituting a Cl^- or Li^+ ion for a methanol molecule in a liquid system consisting of 128 methanol molecules. Polarizable intermolecular potential functions derived by Dang[31] and by Dang et al.[32] were used for the ions. The

periodic boundary condition was employed. As in the case of neat liquid methanol, the time step was set to 2 fs and the temperature was kept at 298 K by adjusting the total kinetic energy every 200 fs. The system was equilibrated for 60 ps, and a production run of 160−240 ps was carried out.

Inspection of the radial distribution function for the Cl^- ion and the hydroxyl hydrogen atom indicated that the first solvation shell of this ion is defined as $r(Cl^-\cdots H_O) \leq 3.2$ Å. Similarly, the first solvation shell of the Li^+ ion is defined as $r(Li^+\cdots O) \leq 3.0$ Å. To obtain the spectral features characteristic of the liquid structures formed around the ions, the methanol molecules in the first solvation shell were treated as active molecules for each instantaneous liquid structure extracted from the MD simulations every 200 fs, and the IR and Raman spectra were calculated for these active molecules by the MD/TDC method and then averaged. For almost all the instantaneous liquid structures, four or five methanol molecules were contained in the first solvation shell of the Cl^- ion, and four methanol molecules in the first solvation shell of the Li^+ ion. Only the spectra in the OH stretching region were calculated. All the diagonal elements of the **F** matrix of the active molecules were assumed to be 6.61 mdyn $Å^{-1}$ amu^{-1}, which corresponds to an unperturbed vibrational wavenumber of 3349 cm^{-1} and is slightly smaller than the value used for neat liquid methanol. This slight difference in the diagonal force constant affects only the absolute wavenumber positions of the IR and Raman bands but not the sign and magnitude of the noncoincidence effect. All the other details of the calculations of the IR and Raman spectra, including the magnitude of the transition dipole of each molecule, were the same as in the case of neat liquid methanol.

C. Ab Initio MO Calculations on Cluster Species. Ab initio MO calculations of IR and Raman spectra were carried out for methanol−Cl^- and methanol−Li^+ cluster species by the following three steps. (1) The methanol molecules in the first solvation shell of the ion and the ion itself were extracted from the above MD simulations every 4−8 ps. The IR and Raman spectra were calculated for these instantaneous liquid structures (60 configurations for methanol−Cl^- and 20 configurations for methanol−Li^+) at the Hartree−Fock (HF) level with the 6-31(+)G** basis set (6-31G** augmented by diffuse functions on the oxygen atoms and the ions). In this way, the results obtained from the MD/TDC and the MO approaches may be directly compared with each other. (2) The structures of the above cluster species were optimized at the HF/6-31(+)G** level. The IR and Raman spectra were calculated for the optimized structures. (3) The structures optimized at the HF/6-31(+)G** level were further optimized at the second-order Møller−Plesset perturbation (MP2) level with the 6-31(+)G** basis set. The IR and Raman spectra were then calculated by using the dipole and polarizability derivatives, which are calculated by the method of Komornicki and McIver,[33] and an approximate vibrational force field, which is obtained from the gradients of the structures displaced along the OH stretching coordinates. This step was not carried out for the clusters containing five methanol molecules because of the limitation of the available computational resources.

The configurations of the methanol molecules in the methanol−Cl^- clusters obtained in steps 2 and 3 were used as initial structures in the geometry optimization of the methanol−e^- clusters. The IR and Raman spectra were calculated for the optimized structures of the latter species at the HF and MP2 levels with the 6-31(++)G** basis set [the 6-31(+)G** basis set augmented by diffuse functions on the hydroxyl hydrogens] by using the same procedures as described above for the methanol−Cl^- cluster species.

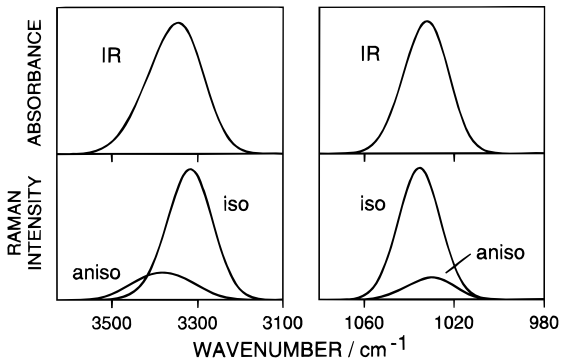

Figure 1. IR and Raman spectra in the OH stretching region (left side) and in the CO stretching region (right side) of neat liquid methanol calculated by the MD/TDC method.

All the ab initio MO calculations were carried out by using the Gaussian 94 program[34] on IBM SP2 computers at the Computer Center of the Institute for Molecular Science and on Hewlett-Packard model 735 and Digital Alpha Station 255/233 workstations at the University of Tokyo.

3. Results and Discussion

A. Neat Liquid Methanol. The IR and Raman spectra of neat liquid methanol in the OH stretching and CO stretching regions calculated by the MD/TDC method are shown in Figure 1. In the OH stretching region, the isotropic Raman component is significantly lower in wavenumber than the anisotropic component ($\Delta\nu_{aniso-iso} > 0$), and the IR band comes near the middle of these two Raman components, in agreement with the experimental results.[17−19] The Raman noncoincidence of the CO stretching band is calculated to be negative ($\Delta\nu_{aniso-iso} < 0$), in accord with the experimental result[16,19] and our previous calculation[8] employing a different set of parameters for the intermolecular potential function.[35] In Table 1, the calculated wavenumbers (first moments) are shown in the row of "all pairs" (i.e., calculated by including vibrational interactions between *all pairs* of molecules). The observed wavenumbers are also shown for comparison. The observed and calculated wavenumbers are in reasonable agreement for all three components of each band.

To examine what kind of intermolecular interactions are important for the wavenumber differences among the IR, isotropic Raman, and anisotropic Raman components, $N(N-1)/2$ pairs of molecules (with N being the number of molecules in the system) are classified into a few categories according to the condition of intermolecular hydrogen bonding and vibrational wavenumbers are calculated by including only the vibrational coupling of the pairs belonging to a given category. In all cases, a common set of liquid structures derived from MD simulations are used. The results are shown in Table 1. A pair of molecules is regarded as hydrogen bonded if the O···H bond length is less than 2.6 Å and the O···H−O angle is larger than 90°.

For the OH stretching band, it is clear from the comparison of the values in the first and fourth rows that the vibrational interactions between hydrogen-bonded pairs of molecules give rise to a major part of the noncoincidence effect (both $\Delta\nu_{aniso-iso}$ and $\Delta\nu_{IR-iso}$). The contribution of the non-hydrogen-bonded pairs [the molecules which are *not directly* hydrogen bonded with each other but *may be* hydrogen bonded with *other* molecules] shown in the second row is rather small. The values

TABLE 1: Calculated and Observed Wavenumbers (first moments, cm^{-1}) of the Infrared and Isotropic/Anisotropic Raman Components of the OH and CO Stretching Bands of Neat Liquid Methanol

	intermolecular interactions	ν_{IR}	ν_{iso}	ν_{aniso}	$\Delta\nu_{IR-iso}$	$\Delta\nu_{aniso-iso}$
			OH stretching band			
calcd[a]	hydrogen-bonded pairs	3354.4	3329.4	3381.0	25.0	51.6
	non-hydrogen-bonded pairs	3386.2	3375.4	3383.8	10.8	8.4
	within hydrogen bond chains	3352.9	3319.0	3380.3	33.9	61.3
	all pairs	3355.8	3320.0	3380.0	35.8	60.0
obsvd[b]		3350	~3320	~3380	~30	~60
			CO stretching band			
calcd[a]	hydrogen-bonded pairs	1032.5	1037.7	1031.2	−5.2	−6.5
	non-hydrogen-bonded pairs	1032.0	1029.2	1031.5	2.8	2.3
	within hydrogen bond chains	1033.1	1037.9	1031.3	−4.8	−6.6
	all pairs	1032.9	1035.4	1031.1	−2.5	−4.3
obsvd[c]			1035.9	1030.9		−5.0
obsvd[d]		1034.7	1034.8	1029.5	−0.1	−5.3

[a] Calculated with the MD/TDC method. [b] References 17−19. [c] Reference 16. [d] Reference 19.

in the third row include the effects of interactions between molecules in a common hydrogen-bonded chain, e.g., between molecules A and C in a hydrogen-bonded chain of A−B−C. For both $\Delta\nu_{aniso-iso}$ and $\Delta\nu_{IR-iso}$, the values in the third row are almost equal to those in the fourth row (the total values). Therefore, it may be said that vibrational interactions within hydrogen-bonded chains explain the major part of the noncoincidence effect of the OH stretching band. This result is in contrast to that obtained in our previous study[28] for the amide I band of liquid formamide, for which only one-third of the total $\Delta\nu_{IR-iso}$ is explained by the vibrational interactions between hydrogen-bonded pairs of molecules.

The situation is different for the CO stretching band. As shown in Table 1, the vibrational interactions between hydrogen-bonded pairs of molecules induce a negative noncoincidence effect, which is partially canceled by the contribution of the non-hydrogen-bonded pairs. In this sense, the vibrational interactions between non-hydrogen-bonded pairs are important for estimating the magnitude of the noncoincidence effect. The partial cancellation originates from the difference in signs between the (average) vibrational coupling constants of hydrogen-bonded pairs and those of non-hydrogen-bonded pairs. As shown in our previous study,[8] the vibrational coupling constants between hydrogen-bonded pairs are mostly positive, giving rise to a negative noncoincidence effect (negative values of $\Delta\nu_{aniso-iso}$ and $\Delta\nu_{IR-iso}$), but the coupling constants between non-hydrogen-bonded pairs are mostly negative, giving rise to a positive noncoincidence effect.

The relation between a coupling constant and the relative orientation of molecules involved in the coupling is shown in Figure 2, parts a and c, for the OH stretching and the CO stretching, respectively, of the hydrogen-bonded pairs of molecules, and parts b and d for those of the non-hydrogen-bonded pairs within 3.8 Å (one molecule in the first solvation shell of the other). The relative orientation of molecules is represented by the scalar product between the unit vectors along the relevant (OH or CO) bond. The number of pairs of molecules is represented by a dot size, with a scale suitable for each part of the figure as indicated in the caption.

As shown in Figure 2a, the scalar products between the unit vectors along the OH bonds are mostly in the range of 0.5−0.9 for hydrogen-bonded pairs of molecules. This is because the OH bonds are arranged in a head-to-tail manner if they are hydrogen bonded to each other. The coupling constants of the OH stretch (given in eq 1) are distributed around −0.1 mdyn $Å^{-1}$ amu^{-1}, giving rise to a large positive noncoincidence effect. The negative values of the coupling constants are consistent with the head-to-tail arrangement of the OH bonds. By contrast,

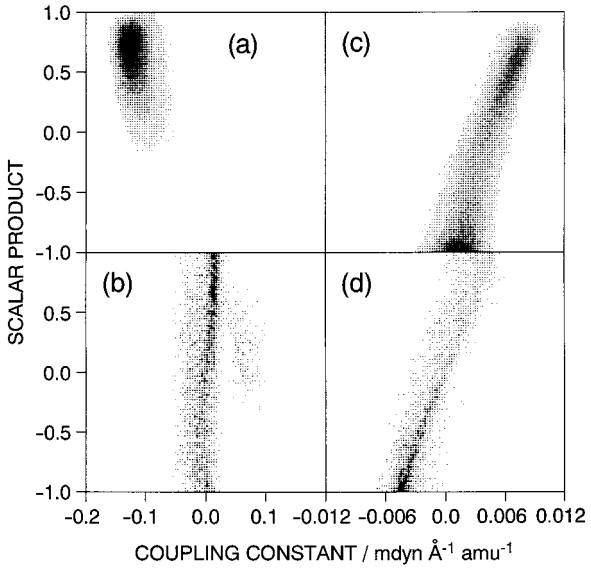

Figure 2. Correlation between a coupling constant and the relative orientation of molecules involved in the coupling for (a) the OH stretching and (c) the CO stretching modes of the hydrogen-bonded pairs of molecules, and for (b) the OH stretching and (d) the CO stretching modes of the non-hydrogen-bonded pairs of molecules within 3.8 Å, in neat liquid methanol. The number of pairs is represented by a dot size. The ratio of the number of pairs represented by the maximum dot size in each figure is (a):(b):(c):(d) = 40:3:26:4.

the scalar products between the unit vectors along the OH bonds are distributed over a wide range for non-hydrogen-bonded pairs of molecules, as shown in Figure 2b. A similar result is obtained for non-hydrogen-bonded pairs with distances larger than 3.8 Å. The contribution of the non-hydrogen-bonded pairs to the noncoincidence effect of the OH stretch is small because the coupling constants are small.

The scalar products between the unit vectors along the CO bonds are distributed over a wide range (from −1.0 to ca. 0.8) even for hydrogen-bonded pairs of molecules as shown in Figure 2c, since hydrogen-bonded molecules have various relative conformations around the O···H hydrogen bond because of structural disorder in the liquid. The coupling constant of the CO stretch is small when the scalar product is negative and is 0.005−0.008 mdyn $Å^{-1}$ amu^{-1} when the scalar product is in the range of 0.3−0.8. Such a positive coupling constant gives rise to a negative noncoincidence effect of the CO stretching band. In other words, the negative noncoincidence effect observed for the CO stretching band indicates the existence of many hydrogen-bonded pairs of molecules with a positive scalar product between the unit vectors along the CO bonds. For non-

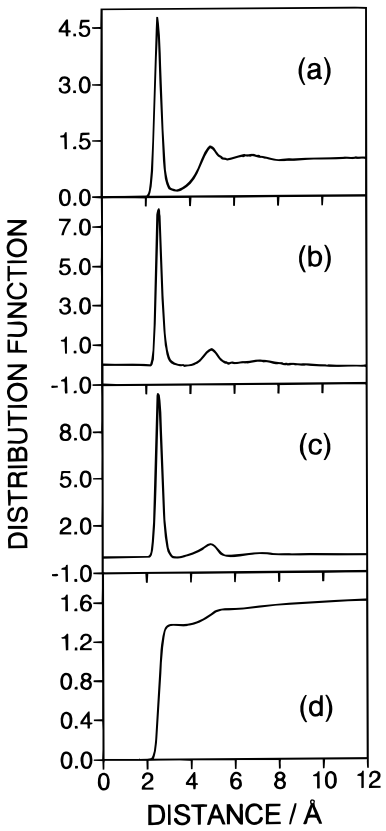

Figure 3. Pair correlation function of the OH bonds in neat liquid methanol: (a) zeroth-order component [$g_0(r)$]; (b) first-order component [$h_\Delta(r)$]; (c) second-order component [$h_D(r)$]; (d) second-order component integrated as given in eq 3 [$H_D(r)$].

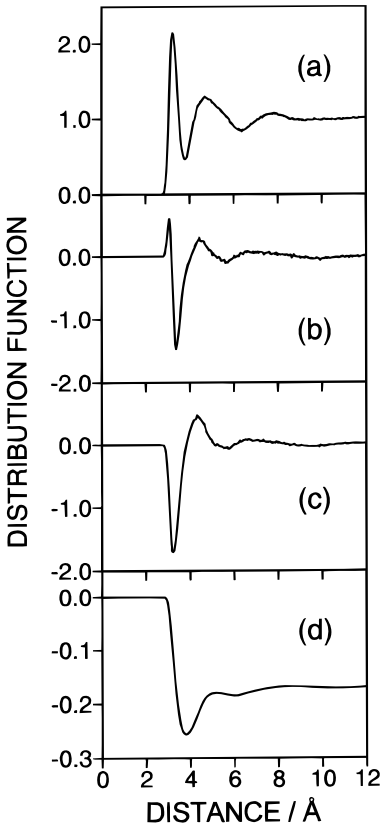

Figure 4. Pair correlation function of the CO bonds in neat liquid methanol: (a) zeroth-order component [$g_0(r)$]; (b) first-order component [$h_\Delta(r)$]; (c) second-order component [$h_D(r)$]; (d) second-order component integrated as given in eq 3 [$H_D(r)$].

hydrogen-bonded pairs of molecules within 3.8 Å, the scalar products between the unit vectors along the CO bonds are mostly negative and the coupling constants are distributed in the range from -0.005 to -0.004 mdyn Å^{-1} amu^{-1}, as shown in Figure 2d. These vibrational interactions partially cancel the negative noncoincidence effect of the CO stretching band. A similar result is obtained when the range of intermolecular distances to be taken into account is extended to 4.5 Å.

To examine the contribution of interacting molecules to the noncoincidence effect as a function of intermolecular distance, the pair distribution functions $g(\mathbf{R}_{ij}; \mathbf{\Omega}_i, \mathbf{\Omega}_j)$ of the OH and CO bonds are evaluated by expanding them to the second order in the form[7,9,36]

$$g(\mathbf{R}_{ij}; \mathbf{\Omega}_i, \mathbf{\Omega}_j) = g_0(R_{ij}) + h_\Delta(R_{ij})\mathbf{\Omega}_i\mathbf{\Omega}_j + h_D(R_{ij})\,[3(\mathbf{R}_{ij}\mathbf{\Omega}_i)(\mathbf{R}_{ij}\mathbf{\Omega}_j)/R_{ij}^{\,2} - \mathbf{\Omega}_i\mathbf{\Omega}_j] \quad (2)$$

where $\mathbf{R}_{ij}$ is the vector connecting the relevant (OH or CO) bonds of molecules i and j, R_{ij} is the length of this vector, and $\mathbf{\Omega}_i$ and $\mathbf{\Omega}_j$ are the unit vectors in the direction of the relevant bonds of the two molecules. In the case where this second-order expansion is a good approximation of $g(\mathbf{R}_{ij}; \mathbf{\Omega}_i, \mathbf{\Omega}_j)$, the Raman noncoincidence ($\Delta\nu_{aniso-iso}$) is proportional to $H_D(\infty)$,[7,9] where the function $H_D(r)$ is defined as[9]

$$H_D(r) = \int_0^r dR\, h_D(R)/R \quad (3)$$

The above four functions ($g_0(r)$, $h_\Delta(r)$, $h_D(r)$, and $H_D(r)$) calculated for the OH and CO bonds of liquid methanol are shown in Figures 3 and 4. In the case of the OH bonds, both $h_\Delta(r)$ and $h_D(r)$ are positive in the $r \leq 3$ Å region as shown in parts b and c of Figure 3, indicating that the OH bonds of hydrogen-bonded molecules are parallel and arranged in a head-to-tail manner. As shown in Figure 3d, a great part of $H_D(\infty)$ is explained by the integration of $h_D(r)/r$ to 3 Å, and a value nearly equal to $H_D(\infty)$ is reached by the integration to about 6 Å. This corresponds to the predominance of the vibrational interactions of the hydrogen-bonded pairs of molecules in the generation of the Raman noncoincidence of the OH stretch, which is shown in the first and third rows of Table 1. By contrast, in the case of the CO bonds, both $h_\Delta(r)$ and $h_D(r)$ are mostly negative in the $r \leq 4$ Å region, and are positive in the 4−5 Å region, as shown in parts b and c of Figure 4. As a result, $H_D(r)$ overshoots the value of $H_D(\infty)$ at $r \cong 4$ Å, and a value nearly equal to $H_D(\infty)$ is reached at $r \cong 5$ Å. This corresponds to the partial cancellation of the hydrogen-bonded and non-hydrogen-bonded pairs of molecules in the generation of the Raman noncoincidence of the CO stretch, which is shown in Table 1.

It should be noted that, for both the OH stretching and the CO stretching bands, the noncoincidence effect is explained by the liquid structures within ca. 6 Å. This conclusion is consistent with that obtained for the C═O stretching band of liquid acetone and acetone/CCl_4 solutions in our previous studies.[9,12]

B. Methanol−Cl^- and Methanol−Li^+ Systems. The IR and Raman spectra in the OH stretching region calculated for the first solvation shell around the ions in methanol−Cl^- and methanol−Li^+ solutions by the MD/TDC method are shown in Figure 5. In the Raman spectra calculated for both solutions [parts b and d of Figure 5], the isotropic component is higher in wavenumber than the anisotropic component. The calculated wavenumbers (first moments) of the IR, isotropic Raman, and anisotropic Raman components are shown in the first part of Table 2. It is clearly seen that the Raman noncoincidence

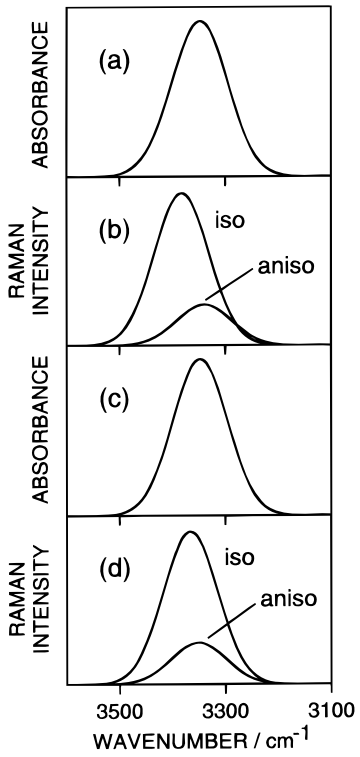

Figure 5. (a) IR and (b) Raman spectra in the OH stretching region calculated for the first solvation shell of the Cl^- ion in a methanol−Cl^- solution, and (c) IR and (d) Raman spectra in the OH stretching region calculated for the first solvation shell of the Li^+ ion in a methanol−Li^+ solution. Calculated by the MD/TDC method.

TABLE 2: Calculated and Observed Wavenumbers (first moments, cm^{-1}) of the Infrared and Isotropic/Anisotropic Raman Components of the OH Stretching Band of the Methanol−LiCl Solution and the Methanol−Cl^- and Methanol−Li^+ Cluster Species

	ν_{IR}	ν_{iso}	ν_{aniso}	$\Delta\nu_{IR-iso}$	$\Delta\nu_{aniso-iso}$
	Calculated (MD/TDC)[a]				
Cl^- in methanol	3348.7	3382.2	3340.5	−33.5	−41.7
Li^+ in methanol	3347.8	3366.1	3350.8	−18.3	−15.3
	Calculated (MO) [b]				
Cl^- + 4 methanol	3340.0	3376.7	3340.7	−36.7	−36.0
Cl^- + 5 methanol	3352.7	3387.0	3353.9	−34.3	−33.1
Li^+ + 4 methanol	3397.3	3397.9	3397.2	−0.6	−0.7
	Observed[c]				
methanol−LiCl solution		3385	3341		−44

[a] Only the solvent molecules in the first solvation shell of the ion are included in the calculations. [b] Structures are directly taken from MD. Calculated at the HF/6-31(+)G** level. Uniformly scaled by 0.815. [c] Reference 18. LiCl/methanol mole ratio of 0.18.

$\Delta\nu_{aniso-iso}$ of −44 cm^{-1} observed for a methanol−LiCl solution,[18] shown in the third part of Table 2, is well reproduced by the calculation for the first solvation shell around the Cl^- ion. This result suggests that the liquid structures formed around the Cl^- ion and the vibrational interactions determined by the TDC mechanism are mainly responsible for the observed Raman noncoincidence effect. It is predicted from the results in Figure 5 and Table 2 that a negative IR−Raman noncoincidence (a negative value of $\Delta\nu_{IR-iso}$) is observed for the methanol−LiCl solution.

The relation between a coupling constant and the relative orientation of molecules involved in the coupling is shown in Figure 6. In the same way as in Figure 2a, the relative orientation of molecules is represented by the scalar product between the unit vectors along the OH bonds, and the number of pairs of molecules is represented by a dot size.

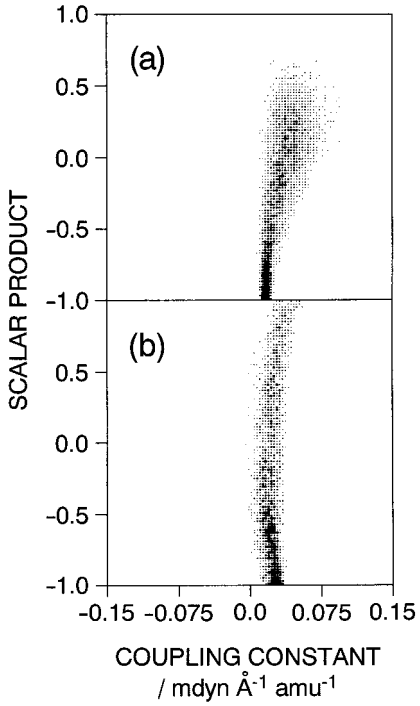

Figure 6. Correlation between a coupling constant of OH stretching vibrations and the relative orientation of the OH bonds of molecules involved in the coupling (a) for pairs of molecules in the first solvation shell of the Cl^- ion and (b) for pairs of molecules in the first solvation shell of the Li^+ ion. The number of pairs is represented by a dot size. The ratio of the number of pairs represented by the maximum dot size in each figure is (a):(b) = 4:3.

As shown in Figure 6a, the scalar products between the unit vectors along the OH bonds are distributed in the range from −1.0 to 0.5 for the methanol molecules around the Cl^- ion, and the coupling constants are significantly positive for some pairs of molecules with scalar products larger than −0.5. This result is rationalized by considering the liquid structures formed around the Cl^- ion. As stated in section 2.B, four or five methanol molecules are contained in the first solvation shell of the Cl^- ion. A typical configuration of methanol molecules around the Cl^- ion (a case of four methanol molecules in the first solvation shell) is shown in Figure 7a. The TDC constants (given by eq 1) between the OH stretches of molecules in such a tetrahedral arrangement are positive. The positive coupling constants of vibrations give rise to negative values of $\Delta\nu_{IR-iso}$ and $\Delta\nu_{aniso-iso}$. It is considered that the broad distribution of the scalar products and the coupling constants shown in Figure 6a arises from disorder in the liquid structures around the Cl^- ion.

As shown in Figure 6b, for methanol molecules around the Li^+ ion, the scalar products between the unit vectors along the OH bonds are distributed in a wider range and the coupling constants are smaller. A typical configuration of methanol molecules around the Li^+ ion is shown in Figure 7b. Since the hydroxyl hydrogen atom of a methanol molecule does not interact directly with the ion, the OH bonds of the methanol molecules around the ion are not in a specific arrangement. As a result, the OH bonds are distributed in a wide range and the coupling constants of the OH stretches are small.

To support the discussion described above, ab initio MO calculations of IR and Raman spectra are carried out for methanol−Cl^- and methanol−Li^+ clusters. As described in

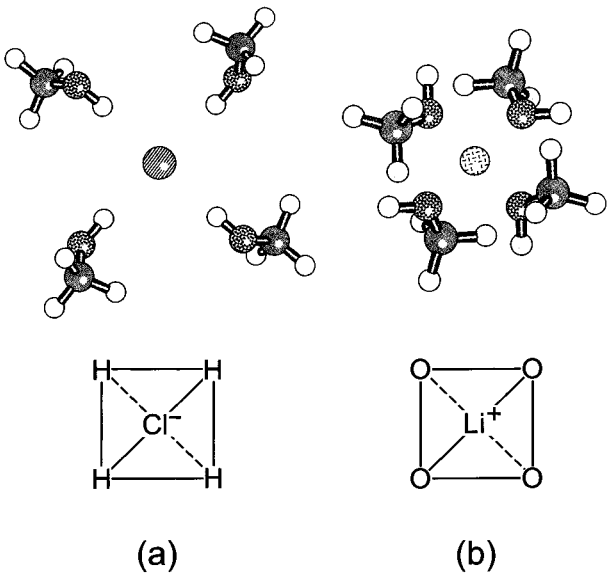

Figure 7. Typical configuration of methanol molecules around (a) the Cl^- ion and (b) the Li^+ ion.

section 2.C, in step 1 of the calculations, the methanol molecules in the first solvation shell of the ion and the ion itself are extracted from the MD simulations. Four OH stretching normal modes are obtained for a cluster containing four methanol molecules, and five modes for that containing five methanol molecules, as in the case of formamide clusters treated in our previous study.[28] Each mode has distinct intensities of the IR, isotropic Raman, and anisotropic Raman components. The intensity of the isotropic Raman component is strong for a normal mode in which all the OH bonds in a cluster stretch in phase, and the intensities of the IR and anisotropic Raman components are strong for some of the other normal modes. The weighted average of the wavenumbers is calculated for each of the three components. In the case of the methanol−Cl^- clusters, the averaging is separately carried out for the clusters containing four methanol molecules and those containing five methanol molecules. The results are shown in the second part of Table 2. It is clearly seen that large negative values of $\Delta\nu_{IR-iso}$ and $\Delta\nu_{aniso-iso}$ are obtained for the methanol−Cl^- clusters, and the values for the methanol−Li^+ clusters are smaller. These results support the conclusion that the liquid structures formed around the Cl^- ion are mainly responsible for the large negative Raman noncoincidence observed for a methanol−LiCl solution.

The wavenumbers calculated for the methanol−Cl^- clusters at their minimum energy structures (in steps 2 and 3 as described in section 2.C) are shown in Table 3. Three and five different structures are obtained, respectively, for the clusters containing four and five methanol molecules. One of these minimum energy structures (structure II of Cl^- + 4 methanol at the HF/6-31(+)G** level) is depicted in Figure 7a. The configurations of the methanol molecules and the potential energies of all the minimum energy structures (in each category of Cl^- + 4 methanol or Cl^- + 5 methanol) are similar to each other. Some of these structures may not be real local minima but artifacts in the calculations due to, for example, a limited size of the basis set used. It should be noted, however, that similar vibrational wavenumbers are calculated for all the minimum energy structures irrespective of the slight structural differences. It is also remarked that the clusters with the Cl^- ion on the surface are not treated, because the purpose of the present study is to discuss the origin of the vibrational spectroscopic features observed in solution.

As shown in Table 3, large negative values are obtained again for $\Delta\nu_{IR-iso}$ and $\Delta\nu_{aniso-iso}$, indicating that the configurations of methanol molecules around the Cl^- ion give rise to a negative noncoincidence effect. The following two points are noteworthy. (1) The values of $\Delta\nu_{IR-iso}$ and $\Delta\nu_{aniso-iso}$ calculated for the minimum energy structures at the HF/6-31(+)G** level are smaller in magnitude than those in Table 2, although the vibrational wavenumbers are calculated at the same theoretical level. It may be said that disorder in the liquid structures is also important for the noncoincidence effect, as in the case of the amide I band of liquid formamide treated in our previous study.[28] (2) The calculations at the MP2/6-31(+)G** level give larger values of $\Delta\nu_{IR-iso}$ and $\Delta\nu_{aniso-iso}$ than those at the HF/6-31(+)G** level. This result indicates that the effect of electron correlation is also important for determining the magnitude of the noncoincidence effect.

For the methanol−Li^+ clusters at their minimum energy structures, very small values of $\Delta\nu_{IR-iso}$ and $\Delta\nu_{aniso-iso}$ are obtained (not shown). This result indicates that the contribution of the structures formed around the Li^+ ion to the noncoincidence effect is small.

C. Solvated Electron in Methanol. As an extension of the analysis described above for the methanol−Cl^- clusters, the IR and Raman spectra in the OH stretching region are calculated for the methanol−e^- clusters. The purpose of this study is to examine possible vibrational spectroscopic features of the liquid structures formed around a solvated electron in solution.

TABLE 3: Calculated Relative Potential Energies (cm^{-1}) and Wavenumbers (first moments, cm^{-1}) of the Infrared and Isotropic/Anisotropic Raman Components of the OH Stretching Band of the Methanol−Cl^- Cluster Species at their Minimum Energy Structures

species	structure no.	ΔE	ν_{IR}	ν_{iso}	ν_{aniso}	$\Delta\nu_{IR-iso}$	$\Delta\nu_{aniso-iso}$
			HF/6-31(+)G** level[a]				
Cl^- + 4 methanol	I	8.0	3346.9	3362.2	3347.0	−15.3	−15.2
	II	0.0	3346.9	3362.5	3348.8	−15.6	−13.7
	III	14.5	3347.2	3362.7	3348.9	−15.5	−13.8
Cl^- + 5 methanol	I	4.0	3370.0	3387.6	3370.3	−17.6	−17.3
	II	0.0	3369.6	3387.4	3370.3	−17.8	−17.1
	III	1.3	3370.3	3387.9	3370.6	−17.6	−17.3
	IV	14.0	3370.4	3388.1	3371.1	−17.7	−17.0
	V	11.5	3370.3	3388.0	3371.2	−17.7	−16.8
			MP2/6-31(+)G** level[b]				
Cl^- + 4 methanol	I	91.6	3350.2	3383.2	3351.4	−33.0	−31.8
	II	3.3	3350.1	3383.0	3357.2	−32.9	−25.8
	III	0.0	3350.1	3382.8	3357.0	−32.7	−25.8

[a] Vibrational wavenumbers are uniformly scaled by 0.83. [b] Calculated by using an approximate vibrational force field. Vibrational wavenumbers are uniformly scaled by 0.92. See text in section 2.C.

TABLE 4: Calculated Relative Potential Energies (cm^{-1}) and Wavenumbers (first moments, cm^{-1}) of the Infrared and Isotropic/Anisotropic Raman Components of the OH Stretching Band of the $e^- + 4$ Methanol Cluster Species at its Minimum Energy Structures

structure no.	ΔE	ν_{IR}	ν_{iso}	ν_{aniso}	$\Delta\nu_{IR-iso}$	$\Delta\nu_{aniso-iso}$
			HF/6-31(++)G** level[a]			
I	0.0	3417.1	3422.3	3417.2	−5.2	−5.1
II	41.4	3416.0	3422.1	3416.6	−6.1	−5.4
			MP2/6-31(++)G** level[b]			
I	0.0	3428.2	3442.1	3428.1	−13.9	−14.0
II	8.2	3428.1	3442.0	3427.9	−13.9	−14.1

[a] Vibrational wavenumbers are uniformly scaled by 0.83. [b] Calculated by using an approximate vibrational force field. Vibrational wavenumbers are uniformly scaled by 0.92. See text in section 2.C.

Therefore, clusters with an electron on the surface are not treated. As described in section 2.C, the configurations of the methanol molecules in the optimized structures of the methanol−Cl^- clusters are used as initial structures in the geometry optimization of the methanol−e^- clusters. Since methanol−e^- clusters with one methanol molecule in the second solvation shell (i.e., hydrogen bonded with another methanol molecule) are obtained from the methanol−Cl^- clusters containing five methanol molecules, we treat only the clusters containing four methanol molecules in this section.

Two different minimum energy structures are obtained at both the HF/6-31(++)G** and MP2/6-31(++)G** levels for the methanol−e^- clusters containing four methanol molecules, with all the methanol molecules in the first solvation shell. The vibrational wavenumbers calculated for these structures are shown in Table 4. It is seen that negative values are obtained for both $\Delta\nu_{IR-iso}$ and $\Delta\nu_{aniso-iso}$. The origin of this negative noncoincidence effect is considered to be similar to that described above for the liquid structures formed around the Cl^- ion. The OH bonds in each of these structures of the methanol−e^- clusters are directed toward the center of the cluster, in the same way as in the methanol−Cl^- clusters. We remark that a similar structure has been suggested for anionic water clusters (models of a hydrated electron) from their IR spectra.[37]

It is predicted, therefore, that a negative noncoincidence effect may be observed for liquid structures formed around a tetrahedrally solvated electron. Measurements of the IR and (resonance) Raman spectra of solutions with excess electrons will be interesting in this respect. It may also be said, however, that different spectral features will be observed for different liquid structures formed around solvated electrons. Further studies will be needed to clarify this point.

4. Concluding Remarks

The IR and isotropic/anisotropic Raman noncoincidence is generated as a result of delocalization of vibrational modes over molecules in a liquid.[28] Consequently, the signs and magnitudes of the noncoincidence effect are sensitive to relative orientations of nearby molecules in a liquid and the vibrational interactions between them.[6−9] It has been shown in the present study that the opposite signs of the noncoincidence effect observed[16−19] for the OH and CO stretching bands of liquid methanol are explained by the same set of liquid structures (derived from MD simulations) and the same mechanism of vibrational interactions (the TDC mechanism), and the sign reversal of the Raman noncoincidence of the OH stretching band occurring upon solvation of LiCl in methanol[18] arises from the significant difference between the liquid structures of neat liquid methanol and those formed around the Cl^- ion. As an extension of the study on the methanol−Cl^- system, a possible vibrational spectroscopic feature of liquid structures formed around a solvated electron has been discussed. It is expected that information on the liquid structures formed around solvated ions and molecules, which are important for understanding the role of solvents in various liquid-phase chemical reactions, will be obtained by analyzing vibrational bands of solvents and the corresponding bands of neat liquids.

References and Notes

(1) Fini, G.; Mirone, P. *J. Chem. Soc., Faraday Trans. 2* **1974**, *70*, 1776.
(2) Schindler, W.; Sharko, P. T.; Jonas, J. *J. Chem. Phys.* **1982**, *76*, 3493.
(3) Dybal, J.; Schneider, B. *Spectrochim. Acta A* **1985**, *41*, 691.
(4) Thomas, H. D.; Jonas, J. *J. Chem. Phys.* **1989**, *90*, 4144.
(5) Shelley, V. M.; Yarwood, J. *Chem. Phys.* **1989**, *137*, 277.
(6) McHale, J. L. *J. Chem. Phys.* **1981**, *75*, 30.
(7) Logan, D. E. *Chem. Phys.* **1986**, *103*, 215.
(8) Torii, H.; Tasumi, M. *J. Chem. Phys.* **1993**, *99*, 8459.
(9) Torii, H. *J. Mol. Struct. (THEOCHEM)* **1994**, *311*, 199.
(10) Giorgini, M. G.; Fini, G.; Mirone, P. *J. Chem. Phys.* **1983**, *79*, 639.
(11) Musso, M.; Giorgini, M. G.; Döge, G.; Asenbaum, A. *Mol. Phys.* **1997**, *92*, 97.
(12) Torii, H.; Musso, M.; Giorgini, M. G.; Döge, G. *Mol. Phys.* **1998**, *94*, 821.
(13) Kamoun, M.; Mirone, P. *Chem. Phys. Lett.* **1980**, *75*, 287.
(14) Torii, H.; Tasumi, M. *J. Chem. Phys.* **1992**, *96*, 3379.
(15) Wertheim, M. S. *J. Chem. Phys.* **1971**, *55*, 4291.
(16) Zerda, T. W.; Thomas, H. D.; Bradley, M.; Jonas, J. *J. Chem. Phys.* **1987**, *86*, 3219.
(17) Perchard, C.; Perchard, J. P. *J. Raman Spectrosc.* **1975**, *3*, 277.
(18) Sokolowska, A.; Kecki, Z. *J. Raman Spectrosc.* **1993**, *24*, 331.
(19) Bertie, J. E.; Michaelian, K. H. *J. Chem. Phys.* **1998**, *109*, 6764.
(20) Perchard, J. P. *Chem. Phys. Lett.* **1976**, *44*, 169.
(21) Kecki, Z.; Sokolowska, A. *J. Raman Spectrosc.* **1994**, *25*, 723.
(22) Craig, D. P.; Thirunamachandran, T. *Chem. Phys.* **1989**, *135*, 37.
(23) Gao, J.; Habibollazadeh, D.; Shao, L. *J. Phys. Chem.* **1995**, *99*, 16460.
(24) Ahlström, P.; Wallqvist, A.; Engström, S.; Jönsson, B. *Mol. Phys.* **1989**, *68*, 563.
(25) Evans, D. J. *Mol. Phys.* **1977**, *34*, 317.
(26) Allen, M. P.; Tildesley, D. J. *Computer Simulation of Liquids*; Oxford University Press: Oxford, 1989.
(27) Torii, H.; Tasumi, M. *Bull. Chem. Soc. Jpn.* **1995**, *68*, 128.
(28) Torii, H.; Tasumi, M. *J. Phys. Chem. B* **1998**, *102*, 315.
(29) Eysel, H. H.; Bertie, J. E. *J. Mol. Struct.* **1986**, *142*, 227.
(30) Bertie, J. E.; Zhang, S. L.; Eysel, H. H.; Baluja, S.; Ahmed, M. K. *Appl. Spectrosc.* **1993**, *47*, 1100.
(31) Dang, L. X. *J. Chem. Phys.* **1992**, *96*, 6970.
(32) Dang, L. X.; Rice, J. E.; Caldwell, J.; Kollman, P. A. *J. Am. Chem. Soc.* **1991**, *113*, 2481.
(33) Komornicki, A.; McIver, J. W., Jr. *J. Chem. Phys.* **1979**, *70*, 2014.
(34) Frisch, M. J.; Trucks, G. W.; Schlegel, H. B.; Gill, P. M. W.; Johnson, B. G.; Robb, M. A.; Cheeseman, J. R.; Keith, T.; Petersson, G. A.; Montgomery, J. A.; Raghavachari, K.; Al-Laham, M. A.; Zakrzewski, V. G.; Ortiz, J. V.; Foresman, J. B.; Cioslowski, J.; Stefanov, B. B.; Nanayakkara, A.; Challacombe, M.; Peng, C. Y.; Ayala, P. Y.; Chen, W.; Wong, M. W.; Andres, J. L.; Replogle, E. S.; Gomperts, R.; Martin, R. L.; Fox, D. J.; Binkley, J. S.; Defrees, D. J.; Baker, J.; Stewart, J. J. P.; Head-Gordon, M.; Gonzalez, C.; Pople, J. A. *Gaussian 94*; Gaussian, Inc.: Pittsburgh, PA, 1995.
(35) Jorgensen, W. L. *J. Phys. Chem.* **1986**, *90*, 1276.
(36) Blum, L. *J. Chem. Phys.* **1972**, *57*, 1862.
(37) Bailey, C. G.; Kim, J.; Johnson, M. A. *J. Phys. Chem.* **1996**, *100*, 16782.